DRAFT
CMS Paper

2017/01/10
Head Id: 379991
Archive Id: 379998P
Archive Date: 2017/01/10
Archive Tag: trunk

Measurement of prompt and nonprompt J/ψ production in pp and pPb collisions at $\sqrt{s_{_{\mathrm{NN}}}} = 5.02\,\mathrm{TeV}$

The CMS Collaboration

Abstract

This paper reports the measurement of J/ψ meson production in proton-proton (pp) and proton-lead (pPb) collisions at a center-of-mass energy per nucleon pair of 5.02 TeV by the CMS experiment at the LHC. The data samples used in the analysis correspond to integrated luminosities of 28.0 pb^{-1} and 34.6 nb^{-1} for pp and pPb collisions, respectively. Prompt and nonprompt J/ψ mesons, the latter issuing from the decay of b hadrons, are measured in their dimuon decay channels. Differential cross sections are measured in the transverse momentum range of $2 < p_{\mathrm{T}} < 30\,\mathrm{GeV}/c$, and center-of-mass rapidity ranges of $|y_{\mathrm{CM}}| < 2.4$ (pp) and $-2.87 < y_{\mathrm{CM}} < 1.93$ (pPb). The nuclear modification factor, R_{pPb}, is measured as functions of p_{T} and y_{CM}. Moderate modifications of the prompt J/ψ yields are observed in pPb relative to pp collisions, whereas nonprompt yields are consistent with (properly scaled) pp yields within experimental uncertainties. The ratio of the forward (proton-going direction) and backward (Pb-going direction) prompt and nonprompt J/ψ yields, R_{FB}, studied as functions of p_{T} and y_{CM}, shows a significant decrease for increasing hadronic activity in the pPb event, as given by the transverse energy deposited in the forward pseudorapidity region. These results provide new constraints of cold nuclear matter effects on prompt and nonprompt J/ψ production over a wide kinematical range.

1 Introduction

It was suggested three decades ago that quark-gluon plasma (QGP) formation would suppress the yield of J/ψ mesons in high-energy heavy ion collisions, relative to that in proton-proton (pp) collisions, as a consequence of Debye screening of the heavy-quark potential at finite temperature [1]. This QGP signature triggered intense research activity, both experimental and theoretical, on the topic of heavy quarkonium production in nuclear collisions. Experiments at SPS [2, 3], RHIC [4], and CERN LHC [5, 6] have reported a significant J/ψ suppression for increasingly central heavy ion collisions over a wide range in rapidity (y) and transverse momentum (p_{T}). In addition, a suppression of different bottomonium states [Υ(1S), Υ(2S), Υ(3S)] has been observed at the LHC in lead-lead (PbPb) collisions at a center-of-mass energy per nucleon pair of $\sqrt{s_{_{\mathrm{NN}}}} = 2.76\,\mathrm{TeV}$ [7, 8], which appears to be consistent with the suggested picture of quarkonium suppression in QGP [9, 10].

In order to interpret unambiguously these results, it is necessary to constrain the so-called cold nuclear matter effects on quarkonium production, through baseline measurements in proton-lead (pPb) collisions. Among these effects, parton distribution functions in nuclei (nPDF) are known to differ from those in a free proton and thus influence the quarkonium yields in nuclear collisions. The expected depletion of gluon nuclear density at small values of the momentum fraction (x), an effect known as shadowing, would suppress J/ψ production at forward y, corresponding to the proton-going direction in pPb collisions [11, 12]. It is also shown that gluon radiation induced by parton multiple scattering in the nucleus can lead to p_{T} broadening and coherent energy loss, resulting in a significant forward J/ψ suppression in pPb collisions at all available energies [13, 14]. These phenomena can be quantified by the nuclear modification factor R_{pPb}, i.e. by the ratio of J/ψ yields in pPb collisions over those in pp collisions scaled by the number of nucleons in the Pb ion (A = 208), and by the R_{FB} ratio of J/ψ yields at forward (p-going direction) to backward (Pb-going direction) rapidities.

In addition to prompt J/ψ mesons, directly produced in the primary interaction or from the decay of heavier charmonium states such as ψ(2S) and χ_{c}, production of J/ψ mesons includes a nonprompt contribution coming from the decay of b hadrons, which production rate are also expected to be affected by cold nuclear matter effects. However, no clear modification of their cross sections in pPb collisions has been observed for high-p_{T} B mesons [15], nor for b quark jets [16]. In this respect, the nonprompt component of J/ψ production can shed light on the nature of nuclear effects at low p_{T}, where nuclear effects are expected to be significant.

At the LHC, the yield of J/ψ mesons in pPb collisions at $\sqrt{s_{_{\mathrm{NN}}}} = 5.02\,\mathrm{TeV}$ has been measured by ALICE [17, 18], ATLAS [19], and LHCb [20] collaborations. The R_{FB} has been determined as functions of the rapidity in the center-of-mass frame, y_{CM}, and p_{T}. Using an interpolated pp production cross section at the same collision energy, R_{pPb} has also been estimated in Refs. [17, 18, 20] as functions of y_{CM} and p_{T}. A significant suppression of the prompt J/ψ yield in pPb collisions has been observed at forward y and low p_{T}, while no strong nuclear effects are reported at backward y.

This paper reports the analysis of J/ψ production in pp and pPb collisions at $\sqrt{s_{_{\mathrm{NN}}}} = 5.02\,\mathrm{TeV}$ collected with the CMS detector in 2013 (pPb sample) and in 2015 (pp sample). The J/ψ mesons are measured via their dimuon decay channel over $2 < p_{\mathrm{T}} < 30\,\mathrm{GeV}/c$, and $|y_{\mathrm{CM}}| < 2.4$ in pp, and $-2.87 < y_{\mathrm{CM}} < 1.93$ in pPb collisions. The corresponding values of x range from 10^{-4}, at forward y and low p_{T}, to 10^{-2}, at backward y and higher p_{T}. Both R_{pPb} and R_{FB} are measured as functions of y_{CM} and p_{T}. The latter ratio is also studied as a function of the event activity in pPb collisions, as characterized by the transverse energy deposit in the forward part of the CMS detector.

2 Experimental setup and event selection

The main feature of the CMS detector is a superconducting solenoid with an internal diameter of 6 m, providing a magnetic field of 3.8 T. Within the field volume are the silicon pixel and strip tracker, the crystal electromagnetic calorimeter, and the brass and scintillator hadronic calorimeter. The silicon pixel and strip tracker measures charged particle trajectories in the pseudorapidity range of $|\eta| < 2.5$. It consists of 66 M pixel and 10 M strip sensor elements. Muons are detected in the range of $|\eta| < 2.4$, with detection planes based on three technologies: drift tubes, cathode strip chambers, and resistive plate chambers. The CMS apparatus also has extensive forward calorimetry, including two steel and quartz-fiber Cherenkov hadron forward (HF) calorimeters, which cover $2.9 < |\eta| < 5.2$. These detectors are used for online event selection and the impact parameter characterization of the events in pPb collisions, where the term impact parameter refers to the transverse distance between the two centers of the colliding particles. A more detailed description of the CMS detector, together with a definition of the coordinate system used and the relevant kinematic variables, can be found in Ref. [21].

The pPb data set used in this analysis corresponds to an integrated luminosity of $34.6\,\mathrm{nb}^{-1}$. The beam energies are 4 TeV for protons, and 1.58 TeV per nucleon for the lead nuclei, resulting in $\sqrt{s_{\mathrm{NN}}} = 5.02\,\mathrm{TeV}$. The direction of the higher-energy proton beam was initially set up to be clockwise, and was reversed after $20.7\,\mathrm{nb}^{-1}$. As a result of the beam energy difference, the nucleon-nucleon center-of-mass in pPb collisions is not at rest with respect to the laboratory frame. Massless particles emitted at $|\eta_{\mathrm{CM}}| = 0$ in the nucleon-nucleon center-of-mass frame are detected at $\eta_{\mathrm{lab}} = -0.465$ for the first run period (clockwise proton beam) and $+0.465$ for the second run period (counterclockwise proton beam) in the laboratory frame. The center-of-mass rapidity region $-2.87 < y_{\mathrm{CM}} < 1.93$ is thus probed. The pp data set is also collected at the same collision energy with an integrated luminosity of $28.0\,\mathrm{pb}^{-1}$. In this sample, J/ψ mesons are measured over $|y_{\mathrm{CM}}| < 2.4$.

In order to remove beam related background such as beam-gas interactions, inelastic hadronic collisions are selected by requiring a coincidence of at least one of the HF calorimeter towers with more than 3 GeV of total energy in each side of the interaction point. This requirement is not present in pp collisions which suffer less from photon-induced interaction compared to pPb collisions. The pp and pPb events are further selected to have at least one reconstructed primary vertex composed of two or more associated tracks, within 25 cm from the nominal interaction point along the beam axis and within 2 cm in its transverse plane. To reject beam-scraping events, the fraction of good-quality tracks associated to the primary vertex is required to be larger than 25% when there are more than 10 tracks per event.

In pPb collisions, an additional filter [22] is applied to remove multiple interactions per bunch crossing (pileup). After the selection, the residual fraction of pileup events is reduced from 3% to less than 0.2%. This pileup rejection results in a 4.1% signal loss, which is corrected for in the cross section measurements. Since pileup only affects the event activity dependence in pPb results, no filter is applied in pp results.

Dimuon events are selected by the level-1 trigger, a hardware-based trigger system requiring two muon candidates in the muon detectors with no explicit limitations in momentum or rapidity. Offline, muons are required to be within the following kinematic regions, which ensure single-muon reconstruction efficiencies above 10%:

$$
\begin{aligned}
p_{\mathrm{T}}^{\mu} &> 3.3\,\mathrm{GeV}/c && \text{for } |\eta_{\mathrm{lab}}^{\mu}| < 1.2\,, \\
p_{\mathrm{T}}^{\mu} &> (4.0 - 1.1|\eta_{\mathrm{lab}}^{\mu}|)\,\mathrm{GeV}/c && \text{for } 1.2 \leq |\eta_{\mathrm{lab}}^{\mu}| < 2.1\,, \\
p_{\mathrm{T}}^{\mu} &> 1.3\,\mathrm{GeV}/c && \text{for } 2.1 \leq |\eta_{\mathrm{lab}}^{\mu}| < 2.4\,.
\end{aligned} \tag{1}
$$

The muon pairs are further selected to be of opposite charge, to originate from a common vertex with a χ^2 probability greater than 1%, and to match standard identification criteria [23].

Simulated events are used to obtain the correction factors for acceptance and efficiency. The Monte Carlo (MC) samples of J/ψ mesons are generated using PYTHIA 6.424 [24] for pPb and PYTHIA 8.209 [25] for pp collisions. Generated particles in the pPb simulation are boosted by $\Delta y = \pm 0.465$ to account for the asymmetry of proton and lead beams in the laboratory frame. Samples for prompt and nonprompt J/ψ mesons are independently produced using the D6T [26] and Z2 [27] tunes, respectively. In the absence of experimental information on quarkonium polarization in pPb and pp collisions at $\sqrt{s} = 5.02\,\mathrm{TeV}$, it is assumed that prompt J/ψ mesons are produced unpolarized, as observed in pp collisions at $\sqrt{s} = 7\,\mathrm{TeV}$ [28]. The nonprompt J/ψ sample includes the polarization ($\lambda_\theta \approx -0.4$) determined from a measurement of the exclusive B meson decays ($\mathrm{B}^+, \mathrm{B}^0, \mathrm{B}^0_\mathrm{s}$, and Λ_b) as implemented in EVTGEN 9.1 [29]. The impact in the final cross sections of the different polarization assumptions is not included in the systematic uncertainties, as done in the previous analyses [7, 8]. A quantitative investigation of effects from two extreme scenarios can be found in Ref. [5]. The final-state QED radiation of decayed muons is taken care of using PHOTOS 215.5 [30]. Finally, the CMS detector response is simulated using GEANT4 [31].

3 Analysis procedure

3.1 Differential cross section, R_{pPb}, and R_{FB}

In this paper, three observables analyzed in J/ψ meson decays to muon pairs are reported. First, the cross sections are computed by:

$$
\mathcal{B}(\mathrm{J}/\psi \to \mu^+\mu^-)\frac{\mathrm{d}^2\sigma}{\mathrm{d}p_{\mathrm{T}}\mathrm{d}y_{\mathrm{CM}}} = \frac{N_{\mathrm{Fit}}^{\mathrm{J}/\psi}/(\mathrm{Acc}\,\varepsilon)}{\mathcal{L}_{\mathrm{Int}}\Delta p_{\mathrm{T}}\Delta y_{\mathrm{CM}}}\,, \tag{2}
$$

where $\mathcal{B}(\mathrm{J}/\psi \to \mu^+\mu^-) = 0.0596 \pm 0.0003$ is the branching fraction to the $\mu^+\mu^-$ channel [32], $N_{\mathrm{Fit}}^{\mathrm{J}/\psi}$ is the extracted raw yield of J/ψ mesons in a given ($p_{\mathrm{T}}, y_{\mathrm{CM}}$) bin, ($\mathrm{Acc}\,\varepsilon$) represents the dimuon acceptance times efficiency described in Section 3.3, and $\mathcal{L}_{\mathrm{Int}}$ is the integrated luminosity with the values of $(28.0 \pm 0.6)\,\mathrm{pb}^{-1}$ for pp [33] and $(34.6 \pm 1.2)\,\mathrm{nb}^{-1}$ for pPb [34] collisions.

The cross sections are measured in up to nine bins in p_{T} ([2,3], [3,4] [4,5], [5,6.5], [6.5,7.5], [7.5,8.5], [8.5,10], [10,14], [14,30] GeV/c), with the minimum p_{T} value varying with the rapidity range as shown in Table 1.

The second observable considered is the nuclear modification factor, calculated as

$$
R_{\mathrm{pPb}}(p_{\mathrm{T}}, y_{\mathrm{CM}}) = \frac{(\mathrm{d}^2\sigma/\mathrm{d}p_{\mathrm{T}}\mathrm{d}y_{\mathrm{CM}})_{\mathrm{pPb}}}{\mathrm{A}(\mathrm{d}^2\sigma/\mathrm{d}p_{\mathrm{T}}\mathrm{d}y_{\mathrm{CM}})_{\mathrm{pp}}}\,, \tag{3}
$$

where $\mathrm{A} = 208$ is the atomic mass of the Pb nucleus that appropriately scales up the pp cross sections [35].

Table 1: Rapidity intervals and associated minimum p_{T} values for the J/ψ cross section measurements in pp and pPb collisions.

y_{CM}	Minimum p_{T} (GeV/c)	
	pp	pPb
$1.93 < y_{\mathrm{CM}} < 2.4$	2	N/A
$1.5 < y_{\mathrm{CM}} < 1.93$	4	2
$0.9 < y_{\mathrm{CM}} < 1.5$	6.5	4
$0 < y_{\mathrm{CM}} < 0.9$	6.5	6.5
$-0.9 < y_{\mathrm{CM}} < 0$	6.5	6.5
$-1.5 < y_{\mathrm{CM}} < -0.9$	6.5	6.5
$-1.93 < y_{\mathrm{CM}} < -1.5$	4	5
$-2.4 < y_{\mathrm{CM}} < -1.93$	2	4
$-2.87 < y_{\mathrm{CM}} < -2.4$	N/A	2

The third measurement is the forward-to-backward production ratio for pPb collisions, defined for positive rapidity by:

$$R_{\mathrm{FB}}(p_{\mathrm{T}}, y_{\mathrm{CM}} > 0) = \frac{\mathrm{d}^2\sigma(p_{\mathrm{T}}, y_{\mathrm{CM}})/\mathrm{d}p_{\mathrm{T}}\mathrm{d}y_{\mathrm{CM}}}{\mathrm{d}^2\sigma(p_{\mathrm{T}}, -y_{\mathrm{CM}})/\mathrm{d}p_{\mathrm{T}}\mathrm{d}y_{\mathrm{CM}}}. \quad (4)$$

This variable proves to be a sensitive probe of the dynamics of J/ψ production by comparing nuclear effects in the forward and the backward rapidity hemispheres, since $R_{\mathrm{FB}}(p_{\mathrm{T}}, y_{\mathrm{CM}}) = R_{\mathrm{pPb}}(p_{\mathrm{T}}, y_{\mathrm{CM}})/R_{\mathrm{pPb}}(p_{\mathrm{T}}, -y_{\mathrm{CM}})$. In addition, several uncertainties cancel in the R_{FB} ratio, such as those from the integrated luminosity determination. The minimum p_{T} values for the R_{FB} measurement are 5 GeV/c for $1.5 < |y_{\mathrm{CM}}| < 1.93$, and 6.5 GeV/$c$ for $|y_{\mathrm{CM}}| < 1.5$. The ratio R_{FB} is also analyzed as a function of $E_{\mathrm{T}}^{\mathrm{HF}|\eta|>4}$, the transverse energy deposited in the HF calorimeter within $4 < |\eta| < 5.2$ range, which is related to the collisional impact parameter. In Table 2, the mean value of $E_{\mathrm{T}}^{\mathrm{HF}|\eta|>4}$ and the fraction of events for each bin used in the analysis are computed from minimum bias pPb events.

Table 2: Ranges of forward transverse energy, $E_{\mathrm{T}}^{\mathrm{HF}|\eta|>4}$, their mean values, and associated fractions of pPb events that fall into each category.

$E_{\mathrm{T}}^{\mathrm{HF}|\eta|>4}$ (GeV)	$\langle E_{\mathrm{T}}^{\mathrm{HF}|\eta|>4} \rangle$	Fraction
0–20	9.4	73%
20–30	24.3	18%
30–120	37.2	9%

3.2 Signal extraction

The signal extraction procedure is similar to that in previous CMS analyses of pp [36, 37] and PbPb [5] collisions. The prompt J/ψ mesons are separated from those coming from b hadron decays by virtue of the pseudo-proper decay length, $\ell_{\mathrm{J}/\psi} = L_{xy}\, m_{\mathrm{J}/\psi}/p_{\mathrm{T}}$, where L_{xy} is the transverse distance between the primary and secondary dimuon vertices in the laboratory frame, $m_{\mathrm{J}/\psi}$ is the mass of the J/ψ meson, and p_{T} is the dimuon transverse momentum. For each p_{T}, y_{CM}, and event activity bin, the fraction of nonprompt J/ψ mesons (*b fraction*) is evaluated through an extended unbinned maximum likelihood fit to the invariant mass spectrum and $\ell_{J/\psi}$ distributions of $\mu^+\mu^-$ pairs sequentially.

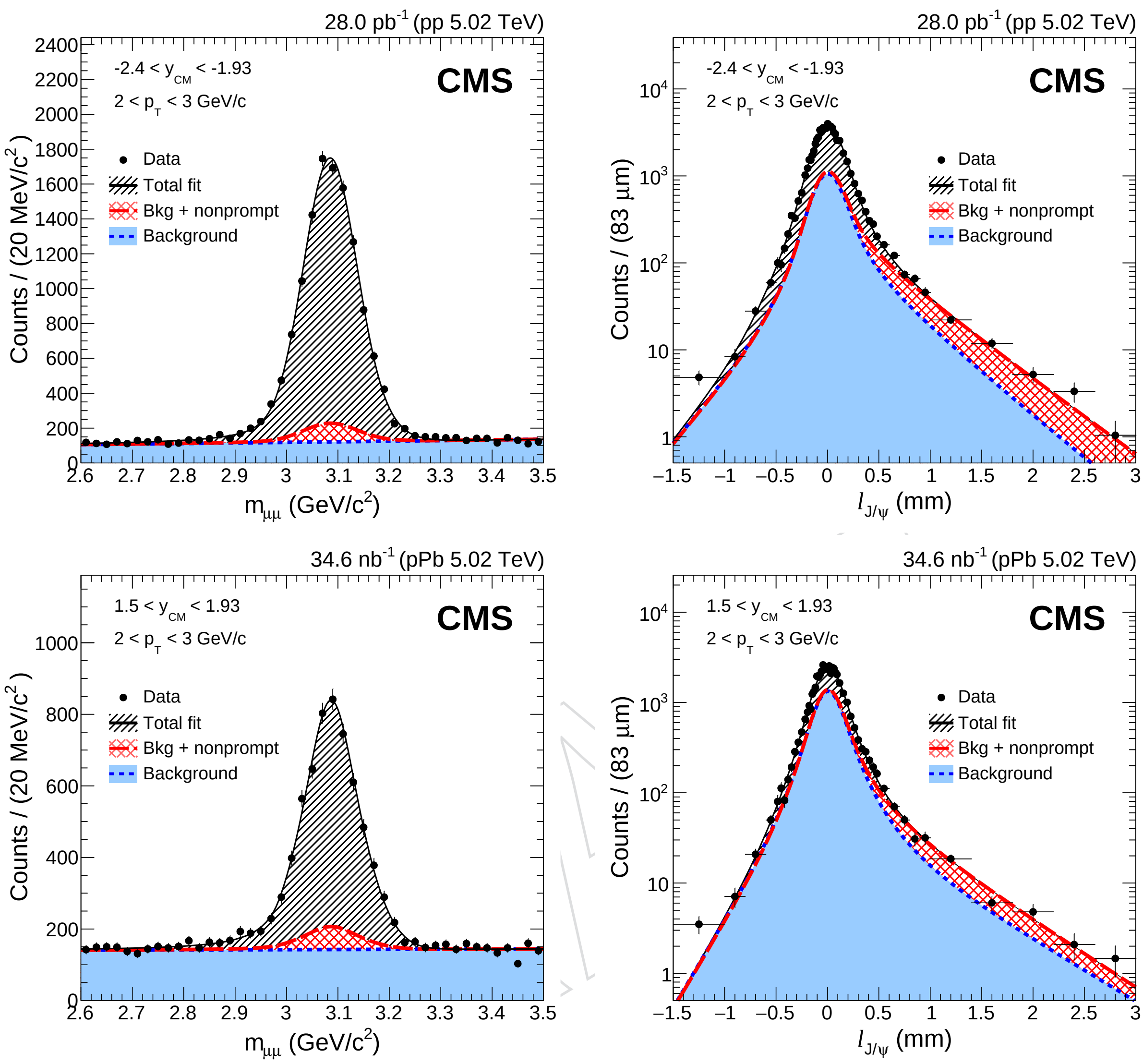

Figure 1: Examples of the invariant mass (left) and pseudo-proper decay length (right) distributions of $\mu^+\mu^-$ pairs for pp (upper) and pPb (lower) collisions. The projections of the 2D fit function onto the respective axes are overlaid as black solid lines. The long-dashed lines show the fitted contribution of nonprompt J/ψ mesons. The fitted background contributions are shown by short-dashed lines.

For the dimuon invariant mass distributions, the shape of the J/ψ signal is modeled by the sum of a Gaussian function and a Crystal Ball (CB) function [38], with common mean values and independent widths, in order to accommodate the rapidity-dependent mass resolution. The CB function combines a Gaussian core with a power-law tail using two parameters n_{CB} and α_{CB}, to describe final-state QED radiation of muons. Because the two parameters are strongly correlated, the $n_{\mathrm{CB}} = 2.1$ is fixed, while α_{CB} is a free parameter of the fit. This configuration gives the highest fit probability for data, in every $(p_{\mathrm{T}}, y_{\mathrm{CM}})$ bin, when various settings of α_{CB} and n_{CB} are tested. The invariant mass distribution of the underlying continuum background is represented by an exponential decay function.

Concerning the $\ell_{J/\psi}$ distributions, the prompt signal component is represented by a resolution function, which depends on the per-event uncertainty in the $\ell_{J/\psi}$ provided by the reconstruction algorithm of primary and secondary vertices. The resolution function is composed of the sum of two Gaussian functions. A Gaussian with a narrower width (σ_{narrow}) describes the core of the signal component, while another with a greater width (σ_{wide}) accounts for the effect of uncertainties in the primary vertex determination and fixed by MC simulation. The $\ell_{J/\psi}$ distribution of the nonprompt component is modeled by an exponential decay function convolved with a resolution function. The continuum background component is reproduced by the sum of three exponential functions, a single-sided left, a single-sided right, and a double-sided, which are also convolved with a resolution function. The parameters describing the $\ell_{J/\psi}$ distributions of the background are determined from sidebands in the invariant mass distribution $2.6 < m_{\mu\mu} < 2.9\,\text{GeV}/c^2$ and $3.3 < m_{\mu\mu} < 3.5\,\text{GeV}/c^2$.

For pPb analysis, two data sets, one corresponding to each beam direction, are merged and fitted together after it is determined the results are compatible when the separate analysis is performed for each data set. Figure 1 shows examples of fit projections onto the mass (left) and $\ell_{J/\psi}$ (right) axes for muon pairs with $2 < p_T < 3\,\text{GeV}/c$ in $-2.4 < y_{\text{CM}} < -1.93$ from pp (upper), and $1.5 < y_{\text{CM}} < 1.93$ from pPb (lower) collisions.

3.3 Corrections

The acceptance and reconstruction, identification, and trigger efficiency corrections are evaluated from the MC simulation described in Section 2. The acceptance is estimated by the fraction of generated J/ψ mesons in the range of $|y| < 2.4$ in the laboratory frame, decaying into two muons, each within the fiducial phase space defined in Eq. 1.

In order to compensate for imperfections in the simulation-based efficiencies, an additional scaling factor is applied, calculated with a *tag-and-probe* (T&P) method [39]. The tag muons require tight identification, and the probe muons are selected with and without satisfying the selection criteria relevant to the efficiency being measured. Then, invariant mass distributions of tag and probe pairs in the J/ψ mass range are fitted to count the number of signals in the two groups. The single-muon efficiencies are deduced from the ratio of J/ψ mesons in the passing probe pair to those in the all probe group. The data-to-simulation ratios of single-muon efficiencies are used to correct the dimuon efficiencies, taking the kinematic distributions of decayed muons into account. The efficiencies are independent of the event activity, as verified by pPb data and in a PYTHIA sample embedded in simulated pPb events generated by HIJING 1.383 [40].

In addition, the shape of uncorrected J/ψ yield distributions in data and MC samples are observed to be different. To resolve the possible bias in acceptance and efficiency corrections, the data-to-simulation ratios are fitted by empirical functions and used to reweight the p_T spectra in MC samples for each y_{CM} bin. The effect of reweighting on the acceptance and efficiency is detailed in Section 3.4.

3.4 Systematic uncertainties

The following sources of systematic uncertainties are considered: fitting procedure, acceptance and efficiency corrections, and integrated luminosities.

To estimate the systematic uncertainty due to the fitting procedure, variations of the parameters or alternative fit functions have been considered for the invariant mass and $\ell_{J/\psi}$ distributions. For the signal shape in the invariant mass distributions, three alternative parameter settings are tested: (1) α_{CB} is set to 1.7, averaged from the default fit, and n_{CB} free, (2) both α_{CB} and

n_{CB} are left free, and (3) both are obtained from an MC template and then fixed when fit to the data. The maximum deviation of yields among these three variations is quoted as the uncertainty. For the background fit functions for the invariant mass distributions, a first-order polynomial is used as an alternative. For the $\ell_{\mathrm{J}/\psi}$ distribution shape of prompt J/ψ mesons, two alternatives are studied: (1) both σ_{wide} and σ_{narrow} are left free, and (2) both parameters are fixed to the MC templates. The maximum deviation of yields is taken as the uncertainty. Finally, for the $\ell_{\mathrm{J}/\psi}$ distribution shape of nonprompt J/ψ mesons, the template shape is directly taken from reconstructed MC events. The uncertainties from the previously mentioned methods are 0.7–5.0% for prompt and 1.1–36.3% for nonprompt J/ψ mesons. They are larger for the shape variations in $\ell_{\mathrm{J}/\psi}$ distributions than in the invariant mass distributions.

For the uncertainties from acceptance and efficiency correction factors, the effect of p_{T} spectra reweighting of the PYTHIA generator as described in Section 3.3 is considered. The deviation of the correction factors obtained from the default PYTHIA spectra and those from data-based weighted spectra is less than 2.9% across all kinematic ranges. The full deviation values are quoted as the systematic uncertainties, which imposes the limits of variances of correction factors upon the pure PYTHIA generator. The determination of uncertainties for T&P corrections is done by propagating the uncertainties in single-muon efficiencies to the dimuon efficiency values. The systematic uncertainties are evaluated by varying the fit conditions in the T&P procedure, and the statistical uncertainties are estimated using a fast parametric simulation. Total uncertainty from T&P corrections is obtained by the quadratic sum of two sources. Uncertainties from the efficiency correction, including the T&P uncertainties, range from 2.4 to 6.1%, and tend to be larger for lower p_{T}. The uncertainty in the integrated luminosities (2.3% for pp [33] and 3.5% for pPb [34]) is global for all points and affects only the production cross sections and R_{pPb}, while it cancels out in the R_{FB} measurements.

Table 3 summarizes the sources of systematic uncertainties considered in this analysis. The range refers to different $(p_{\mathrm{T}}, y_{\mathrm{CM}})$ bins; the uncertainties tend to be lower at high p_{T} and mid y_{CM}, and higher at low p_{T} and forward or backward y_{CM}. The largest uncertainties for nonprompt J/ψ mesons come from the lowest p_{T} bins, 2–3 GeV/c. In the case of the R_{pPb} measurements with the p_{T} limit of 4 GeV/c, maximum uncertainties for nonprompt J/ψ mesons are 12.7% for pp and 12.8% for pPb collisions. The total systematic uncertainty is evaluated as the quadratic sum of the uncertainties from all sources in each kinematic bin, except for those from the integrated luminosity determination.

Table 3: Summary of the relative systematic uncertainties for the cross section measurements, given in percentages, for prompt and nonprompt J/ψ mesons in pp and pPb collisions.

	Prompt J/ψ		Nonprompt J/ψ	
	pp	pPb	pp	pPb
Integrated luminosity	2.3	3.5	2.3	3.5
Signal extraction	0.8–3.2	0.7–5.0	2.0–36.3	1.1–29.5
Acceptance	0.0–2.3	0.0–1.2	0.0–1.3	0.0–1.3
Efficiency	2.4–4.4	2.4–6.1	2.4–4.3	2.4–6.1
Total	2.7–5.3	2.8–7.1	3.4–36.5	3.3–30.1

4 Results

4.1 Prompt J/ψ mesons

Figure 2 shows the double-differential prompt J/ψ production cross sections multiplied by the dimuon branching fraction in pp (left) and pPb (right) collisions, with data points plotted at the center of each bin. Statistical uncertainties are displayed as vertical bars, while boxes represent systematic uncertainties. Not shown is a global normalization uncertainty of 2.3% in pp and 3.5% in pPb collisions arising from the integrated luminosity determination.

Prompt J/ψ rapidity distributions are shown in Fig. 3 in pp (left) and pPb (right) collisions. Data are integrated over two p_T intervals, $6.5 < p_T < 10\,\text{GeV}/c$ (low p_T) and $10 < p_T < 30\,\text{GeV}/c$ (high p_T), shown as circles and squares, respectively.

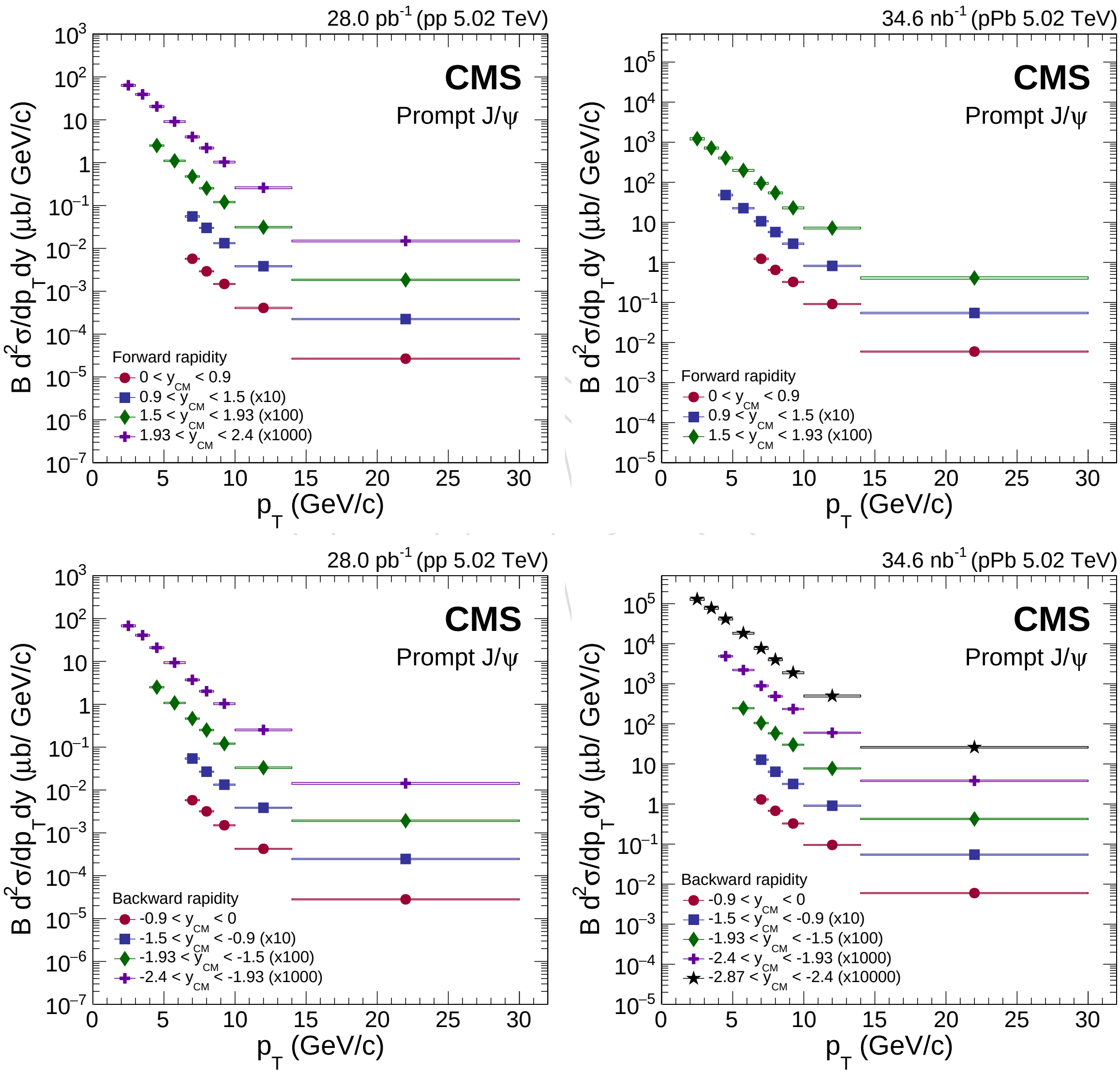

Figure 2: Differential cross section of prompt J/ψ mesons in pp (left) and pPb (right) collisions at forward (upper) and backward (lower) rapidities. The vertical bars represent the statistical uncertainties and the shaded boxes show the systematic uncertainties. The fully correlated global uncertainty, 2.3% for pp and 3.5% for pPb collisions, is not included in the point-by-point uncertainties.

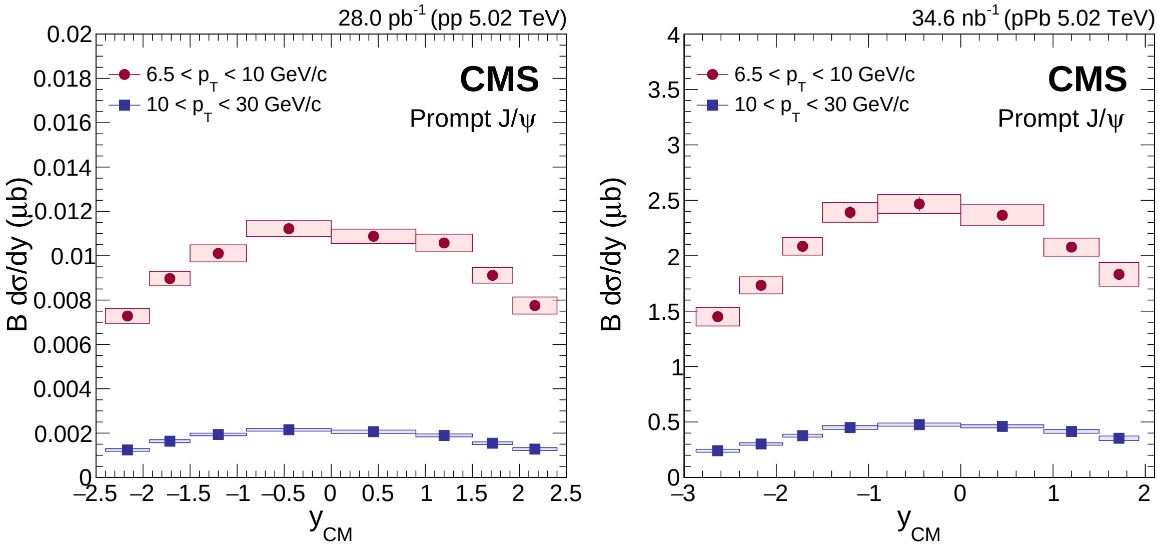

Figure 3: Rapidity dependence of the cross section for prompt J/ψ mesons in the p_T intervals of $6.5 < p_T < 10\,\text{GeV}/c$ (circles) and $10 < p_T < 30\,\text{GeV}/c$ (squares) in pp (left) and pPb (right) collisions. The vertical bars represent the statistical uncertainties, and the shaded boxes show the systematic uncertainties. The fully correlated global uncertainty, 2.3% for pp and 3.5% for pPb collisions, is not included in the point-by-point uncertainties.

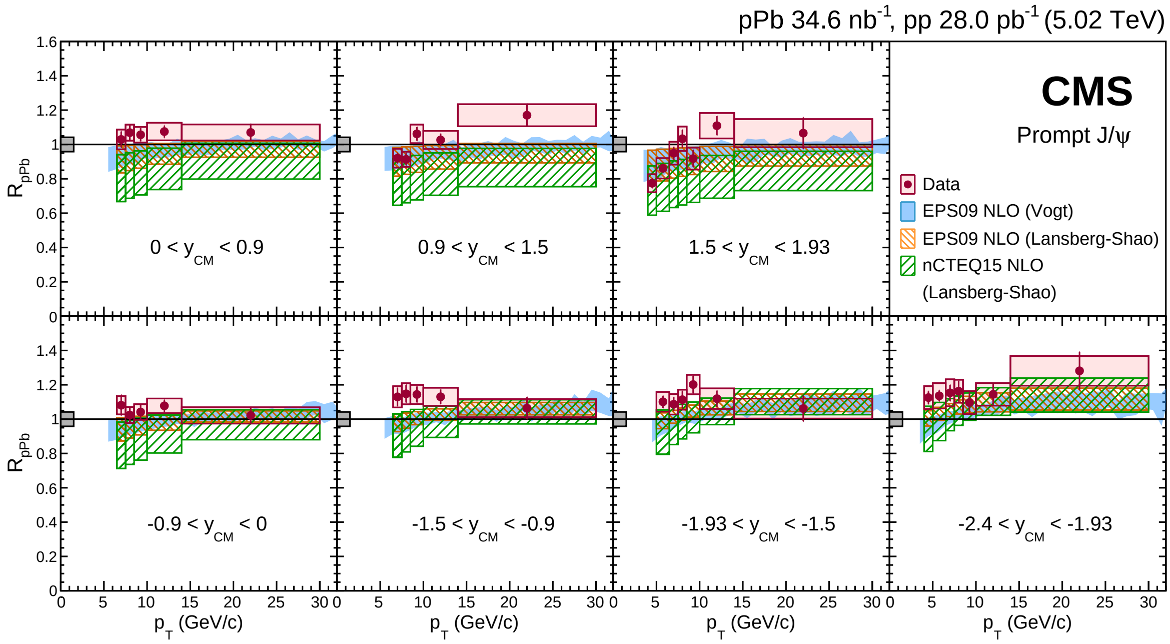

Figure 4: Transverse momentum dependence of R_{pPb} for prompt J/ψ mesons in seven rapidity ranges. The vertical bars represent the statistical uncertainties and the shaded boxes show the systematic uncertainties. The fully correlated global uncertainty of 4.2% is displayed as a gray box at $R_{\mathrm{pPb}} = 1$ near the left axis. The predictions of shadowing models based on the parameterizations EPS09 and nCTEQ15 [12, 41–43] are also shown.

The p_T dependence of R_{pPb} is shown in Fig. 4, in the seven rapidity ranges for which pp and pPb measurements overlap. Around midrapidity ($|y_{CM}| < 0.9$) and in the three backward rapidity bins (lower panels), R_{pPb} is consistent with (yet systematically slightly above) unity without a clear dependence on p_T, indicating little or no nuclear effect on prompt J/ψ production in this rapidity region. In the most forward bin ($1.5 < y_{CM} < 1.93$), suppression at low p_T ($p_T \lesssim 8\,\text{GeV}/c$) is observed, followed by a weak increase of R_{pPb} at higher p_T. The result is compared to three model calculations. One is based on the EPS09 [41] nPDF set with the next-to-leading order (NLO) Color Evaporation Model [12]. The other two are calculated from the nPDF sets of EPS09 and nCTEQ15 [42], respectively, with the parameterization of $2 \to 2$ partonic scattering process based on data, as described in Ref. [43]. All three R_{pPb} calculations are marginally lower than the measured values across all rapidity bins. The calculations based on coherent energy loss are not yet available to describe quarkonium production at large transverse momentum, $p_T \gtrsim m_{J/\psi}$; no comparison of the model [13] with the present data is thus performed.

It is worth noting that the R_{pPb} values measured in the most forward ($1.5 < y_{CM} < 1.93$) and backward ($-2.4 < y_{CM} < -1.93$) regions are consistent, in the overlapping p_T intervals ($4 < p_T < 8\,\text{GeV}/c$), with inclusive J/$\psi$ measurement from the ALICE [17, 18] collaboration performed over $2.03 < y_{CM} < 3.53$ and $-4.46 < y_{CM} < -2.96$ that used an interpolated pp cross section reference.

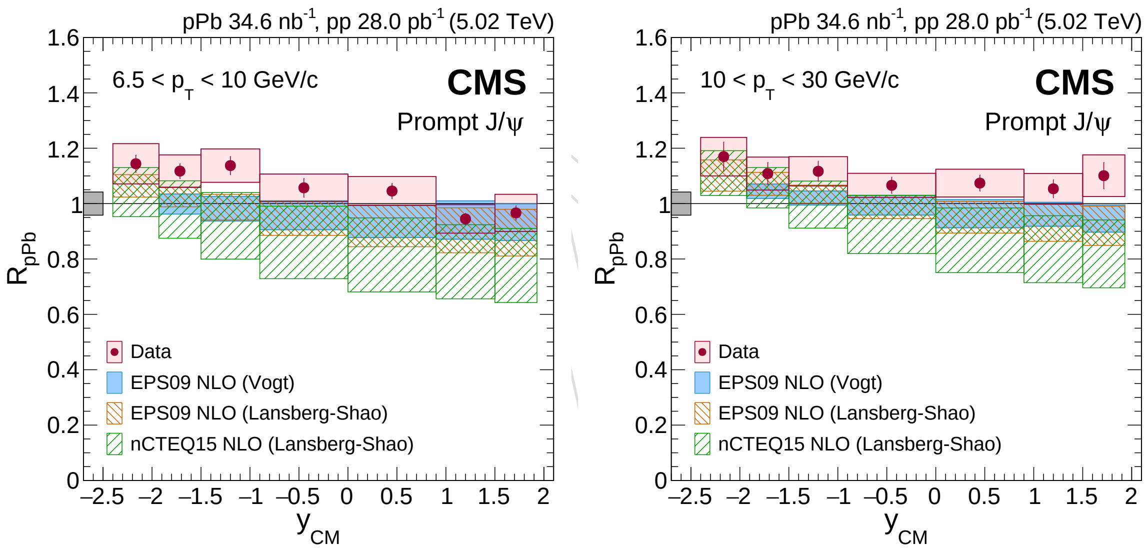

Figure 5: Rapidity dependence of R_{pPb} for prompt J/ψ mesons in two p_T ranges: $6.5 < p_T < 10\,\text{GeV}/c$ (left), and $10 < p_T < 30\,\text{GeV}/c$ (right). The vertical bars represent the statistical uncertainties, and the shaded boxes show the systematic uncertainties. The fully correlated global uncertainty of 4.2% is displayed as a gray box at $R_{pPb} = 1$ near the left axis. The predictions of shadowing models based on the parameterizations EPS09 and nCTEQ15 are also shown [12, 41–43].

Figure 5 displays the rapidity dependence of R_{pPb} in the low-p_T (left) and the high-p_T (right) regions corresponding to the same p_T bins used in Fig. 3. In both p_T regions, R_{pPb} is consistent with (yet slightly above) unity over the whole rapidity range, although a decrease of R_{pPb} for increasing y_{CM} cannot be excluded in the lower-p_T region. The same theoretical predictions shown in Fig. 4 are overlaid. In contrast to the measurement of J/ψ mesons in PbPb collisions [5], no significant modification of yields is observed for overall p_T and rapidity ranges, suggesting that the strong suppression of J/ψ yields in PbPb collisions is an effect of QGP formation.

The forward-to-backward ratio of pPb yields, R_{FB}, in three rapidity ranges is displayed as a function of p_T in Fig. 6. The R_{FB} tends to be below unity at low p_T ($p_T \lesssim 8\,\mathrm{GeV}/c$) and forward y_{CM} ($|y_{CM}| > 0.9$), but consistent with unity within uncertainties. In the $6.5 < p_T < 10\,\mathrm{GeV}/c$ bin, an indication of a modest decrease of R_{FB} with increasing rapidity is observed. The results are in agreement with the ATLAS [19], ALICE [17, 18], and LHCb [20] collaborations.

Figure 7 shows R_{FB} as a function of $E_T^{HF|\eta|>4}$ for prompt J/ψ mesons in three rapidity ranges. The data are integrated over $6.5 < p_T < 30\,\mathrm{GeV}/c$; a lower-$p_T$ bin, $5 < p_T < 6.5\,\mathrm{GeV}/c$, is shown in addition for the most forward-backward interval, $1.5 < |y_{CM}| < 1.93$. The value of R_{FB} decreases as a function of $E_T^{HF|\eta|>4}$, indicating the effects that cause the asymmetry between the forward-to-backward production become significant in events with more hadronic activity.

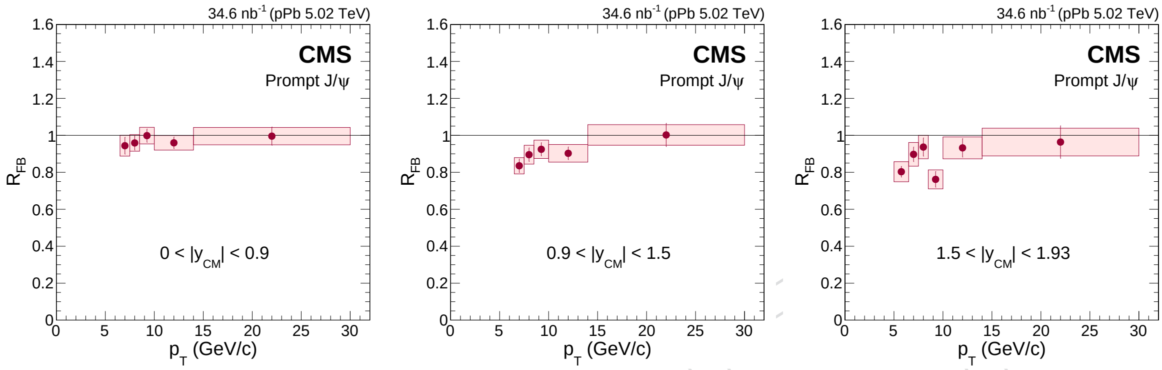

Figure 6: Transverse momentum dependence of R_{FB} for prompt J/ψ mesons in three rapidity regions. The vertical bars represent the statistical uncertainties and the shaded boxes show the systematic uncertainties.

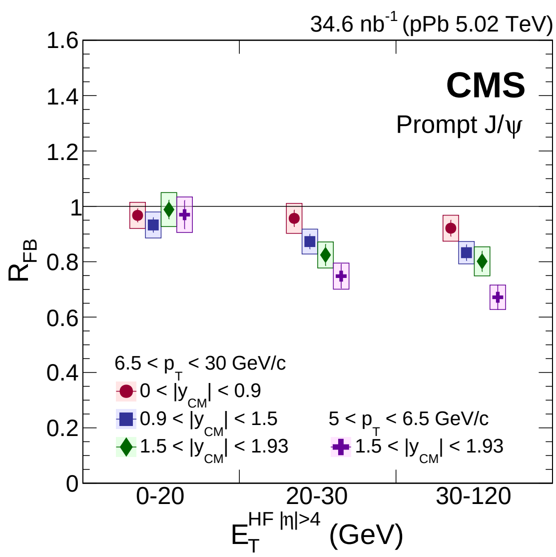

Figure 7: Dependence of R_{FB} for prompt J/ψ mesons on the hadronic activity in the event, given by the transverse energy deposited at forward pseudorapidities $E_T^{HF|\eta|>4}$. The vertical bars represent the statistical uncertainties and the shaded boxes show the systematic uncertainties.

4.2 Nonprompt J/ψ mesons

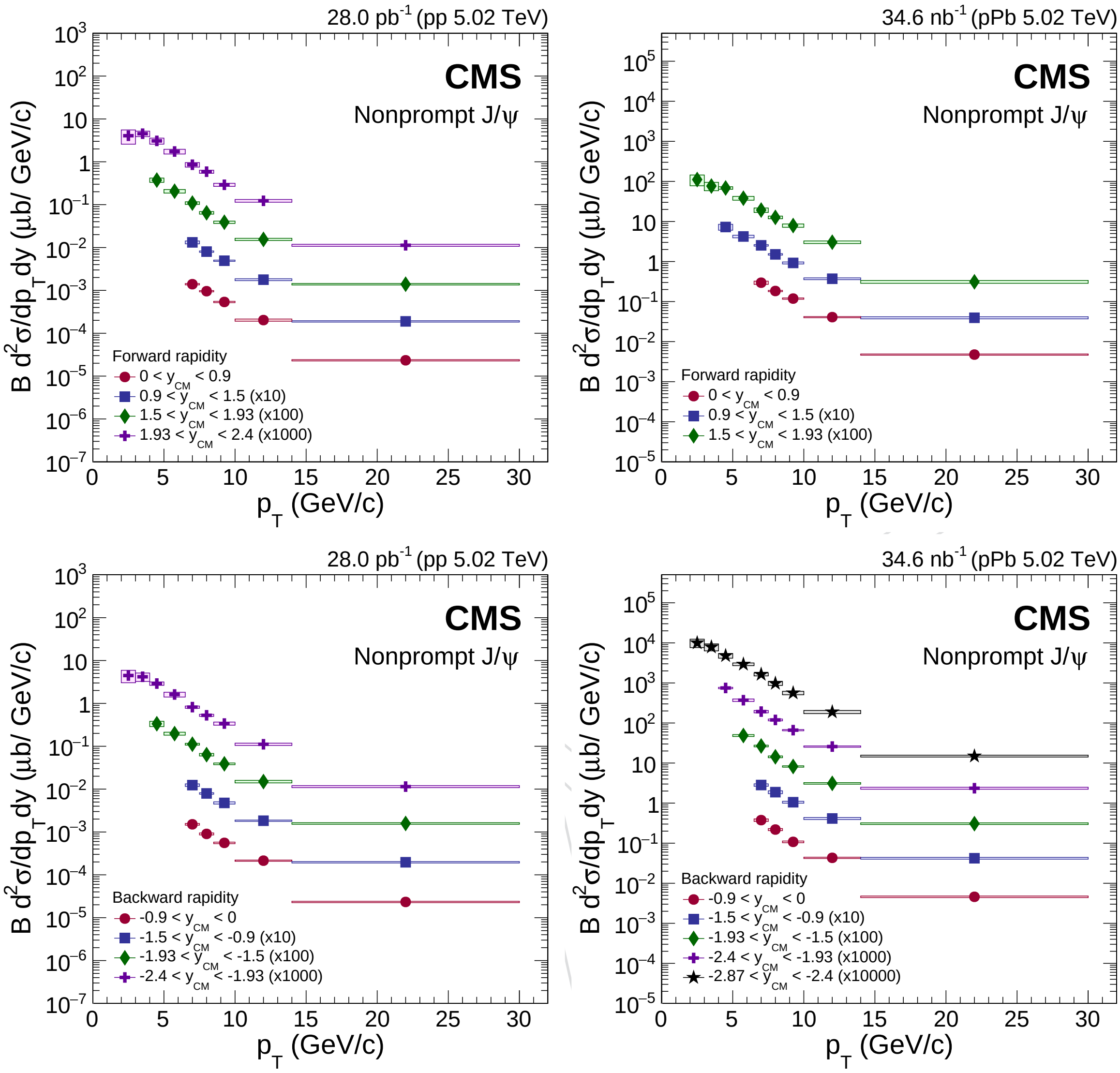

Figure 8: Differential cross section of nonprompt J/ψ mesons in pp (left) and pPb (right) collisions at forward (upper) and backward (lower) rapidities. The vertical bars represent the statistical uncertainties and the shaded boxes show the systematic uncertainties. The fully correlated global uncertainty, 2.3% for pp and 3.5% for pPb, is not included in the point-by-point uncertainties.

The same distributions and observables, as those from Section 4.1, have been investigated in the nonprompt J/ψ meson samples. Differential cross sections are plotted as functions of p_T and y_{CM} in Figs. 8 and 9, respectively, using the same binning as for prompt J/ψ mesons.

The nonprompt J/ψ R_{pPb} plotted in Fig. 10 as a function of p_T is compatible with unity in all rapidity bins, with a possible p_T dependence in the two most backward bins ($y_{CM} < -1.5$). The somewhat larger uncertainties, however, make it difficult to draw firm conclusions for the nonprompt J/ψ production. The rapidity dependence of R_{pPb} integrated in the low- and high-p_T regions is shown in Fig. 11. In all rapidity bins, R_{pPb} is consistent with unity although one cannot exclude a rapidity dependence for R_{pPb} in the low p_T region, as in the prompt J/ψ meson production (Fig. 5).

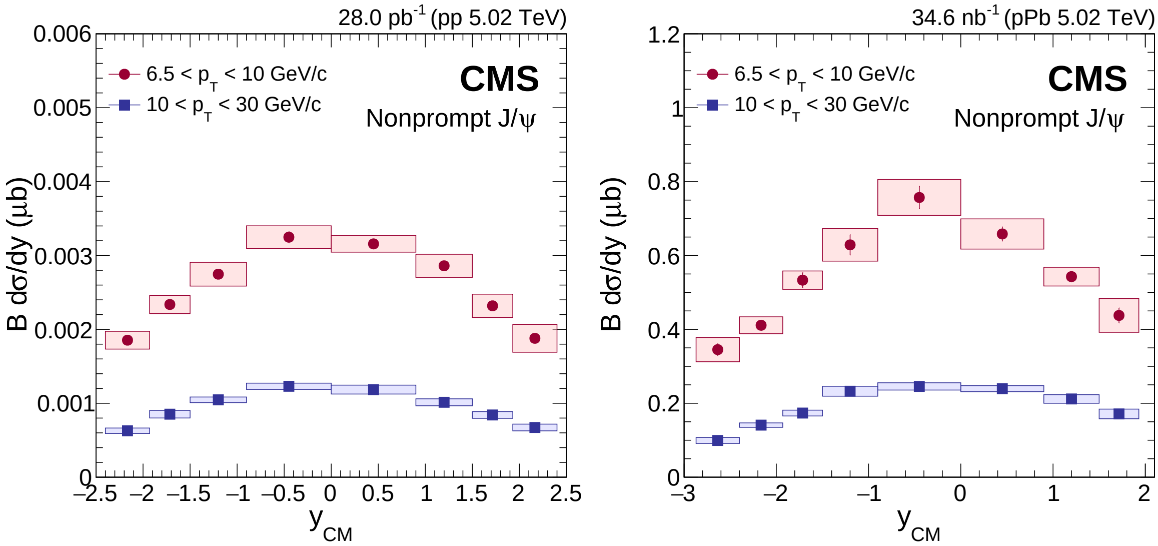

Figure 9: Rapidity dependence of the cross section for nonprompt J/ψ mesons in the p_T intervals of $6.5 < p_T < 10\,\text{GeV}/c$ (circles) and $10 < p_T < 30\,\text{GeV}/c$ (squares) in pp (left) and pPb (right) collisions. The vertical bars represent the statistical uncertainties and the shaded boxes show the systematic uncertainties. The fully correlated global uncertainty, 2.3% for pp and 3.5% for pPb, is not included in the point-by-point uncertainties.

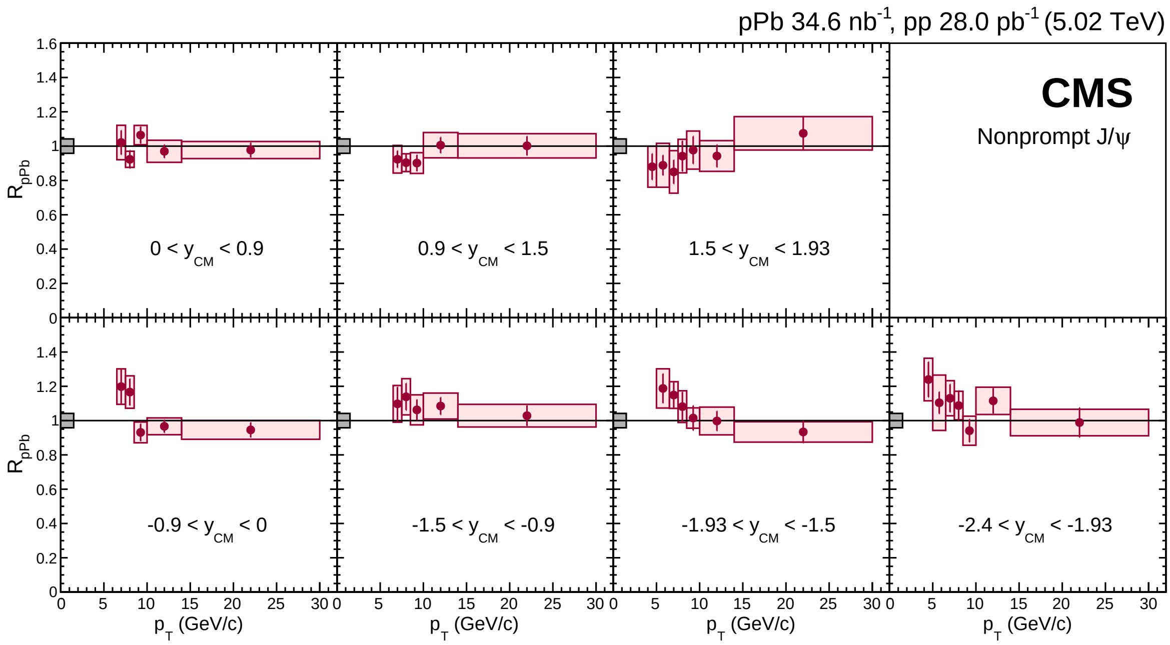

Figure 10: Transverse momentum dependence of R_{pPb} for nonprompt J/ψ mesons in seven rapidity ranges. The vertical bars represent the statistical uncertainties and the shaded boxes show the systematic uncertainties. The fully correlated global uncertainty of 4.2% is displayed as a gray box at $R_{\mathrm{pPb}} = 1$ near the left axis.

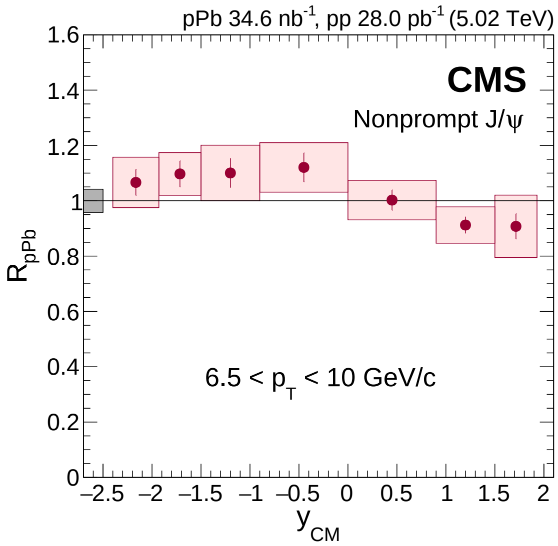

Figure 11: Rapidity dependence of R_{pPb} for nonprompt J/ψ mesons in two p_{T} ranges: $6.5 < p_{\mathrm{T}} < 10\,\mathrm{GeV}/c$ (left), and $6.5 < p_{\mathrm{T}} < 10\,\mathrm{GeV}/c$ (right). The vertical bars represent the statistical uncertainties and the shaded boxes show the systematic uncertainties. The fully correlated global uncertainty of 4.2% is displayed as a gray box at $R_{\mathrm{pPb}} = 1$ near the left axis.

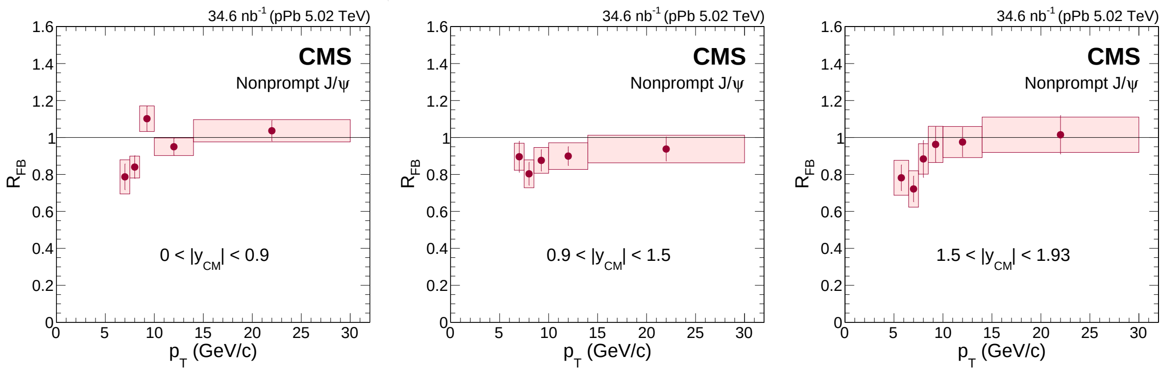

Figure 12: Transverse momentum dependence of R_{FB} for nonprompt J/ψ mesons in three rapidity ranges. The vertical bars represent the statistical uncertainties and the shaded boxes show the systematic uncertainties.

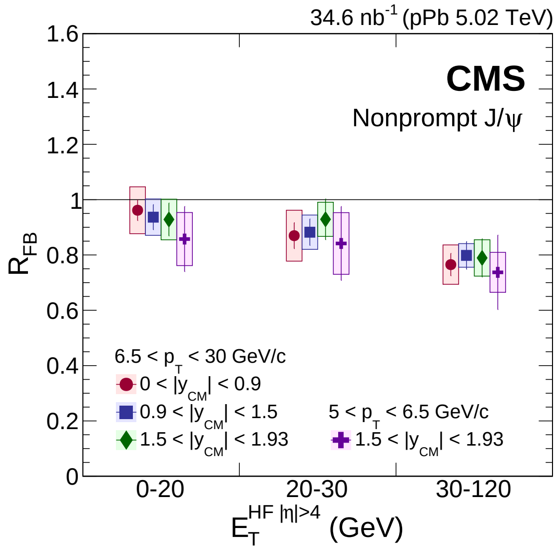

Figure 13: Dependence of R_{FB} for nonprompt J/ψ mesons on the hadronic activity in the event, given by the transverse energy deposited at forward pseudorapidities $E_T^{HF|\eta|>4}$. The vertical bars represent the statistical uncertainties and the shaded boxes show the systematic uncertainties.

Figures 12 and 13 show the p_T and $E_T^{HF|\eta|>4}$ dependence of R_{FB}, respectively. A hint of the increase of R_{FB} with p_T can be seen, in all rapidity bins, with values of R_{FB} compatible with unity in the largest p_T bin. The results are consistent with those of ATLAS [19] and LHCb [20] collaborations within uncertainties. As in the prompt J/ψ meson production, R_{FB} decreases with $E_T^{HF|\eta|>4}$, indicating different nuclear effects at forward than at backward rapidities in the events with the greatest event activity.

5 Summary

The proton-proton (pp) and proton-lead (pPb) data at $\sqrt{s_{\mathrm{NN}}} = 5.02\,\mathrm{TeV}$ collected with the CMS detector are used to investigate the production of prompt and nonprompt J/ψ mesons and their possible modifications due to cold nuclear matter effects. Double-differential cross sections, as well as the nuclear modification factor R_{pPb} and forward-to-backward production ratio R_{FB}, are reported as functions of the transverse momentum, p_{T}, and the center-of-mass rapidity, y_{CM}, of J/ψ mesons.

The R_{pPb} for prompt J/ψ mesons is consistent with unity for $p_{\mathrm{T}} > 6.5\,\mathrm{GeV}/c$ in all y_{CM} intervals analyzed, with a possible depletion in the most forward bin at low $p_{\mathrm{T}} \lesssim 8\,\mathrm{GeV}/c$. In the case of nonprompt J/ψ meson production, R_{pPb} is compatible with unity in all rapidity bins. The prompt J/ψ R_{FB} is below unity at $5 < p_{\mathrm{T}} < 6.5\,\mathrm{GeV}/c$ in the most forward bin, $1.5 < |y_{\mathrm{CM}}| < 1.93$, but is consistent with unity for $p_{\mathrm{T}} \gtrsim 10\,\mathrm{GeV}/c$. A similar trend is observed for the nonprompt J/ψ production in the same bin, within slightly larger uncertainties. The dependence of R_{FB} on the hadronic activity in pPb events has been studied through the variable $E_{\mathrm{T}}^{\mathrm{HF}|\eta|>4}$, characterizing the transverse energy deposited in the forward pseudorapidity region of $4 < |\eta| < 5.2$. The ratio is observed to decrease with increasing event activity for both prompt and nonprompt J/ψ mesons, indicating enhanced cold nuclear matter effects for increasingly central pPb collisions.

A depletion of prompt J/ψ mesons in pPb collisions (as compared to pp collisions) is expected in the forward rapidity region, because of the shadowing of nuclear parton distributions and/or coherent energy loss effects. Such a suppression is seen in the present data at $y_{\mathrm{CM}} > 1.5$ and $p_{\mathrm{T}} \lesssim 8\,\mathrm{GeV}/c$, but not at larger p_{T}, possibly because of the reduced impact of nuclear parton distributions and coherent energy loss effects for increasing J/ψ transverse momenta. At negative rapidity, both effects are known to lead to small nuclear modifications [11–14], as confirmed by the present measurements. Such processes are also expected to affect the nuclear dependence of B meson production and thereby nonprompt J/ψ production [44]. The measurements presented here provide new constraints on cold nuclear matter effects on prompt and nonprompt J/ψ production over a wide kinematical range.

Acknowledgments

We congratulate our colleagues in the CERN accelerator departments for the excellent performance of the LHC and thank the technical and administrative staffs at CERN and at other CMS institutes for their contributions to the success of the CMS effort. In addition, we gratefully acknowledge the computing centers and personnel of the Worldwide LHC Computing Grid for delivering so effectively the computing infrastructure essential to our analyses. Finally, we acknowledge the enduring support for the construction and operation of the LHC and the CMS detector provided by the following funding agencies: the Austrian Federal Ministry of Science, Research and Economy and the Austrian Science Fund; the Belgian Fonds de la Recherche Scientifique, and Fonds voor Wetenschappelijk Onderzoek; the Brazilian Funding Agencies (CNPq, CAPES, FAPERJ, and FAPESP); the Bulgarian Ministry of Education and Science; CERN; the Chinese Academy of Sciences, Ministry of Science and Technology, and National Natural Science Foundation of China; the Colombian Funding Agency (COLCIENCIAS); the Croatian Ministry of Science, Education and Sport, and the Croatian Science Foundation; the Research Promotion Foundation, Cyprus; the Secretariat for Higher Education, Science, Technology and Innovation, Ecuador; the Ministry of Education and Research, Estonian Research Council via IUT23-4 and IUT23-6 and European Regional Development Fund, Estonia;

the Academy of Finland, Finnish Ministry of Education and Culture, and Helsinki Institute of Physics; the Institut National de Physique Nucléaire et de Physique des Particules / CNRS, and Commissariat à l'Énergie Atomique et aux Énergies Alternatives / CEA, France; the Bundesministerium für Bildung und Forschung, Deutsche Forschungsgemeinschaft, and Helmholtz-Gemeinschaft Deutscher Forschungszentren, Germany; the General Secretariat for Research and Technology, Greece; the National Scientific Research Foundation, and National Innovation Office, Hungary; the Department of Atomic Energy and the Department of Science and Technology, India; the Institute for Studies in Theoretical Physics and Mathematics, Iran; the Science Foundation, Ireland; the Istituto Nazionale di Fisica Nucleare, Italy; the Ministry of Science, ICT and Future Planning, and National Research Foundation (NRF), Republic of Korea; the Lithuanian Academy of Sciences; the Ministry of Education, and University of Malaya (Malaysia); the Mexican Funding Agencies (BUAP, CINVESTAV, CONACYT, LNS, SEP, and UASLP-FAI); the Ministry of Business, Innovation and Employment, New Zealand; the Pakistan Atomic Energy Commission; the Ministry of Science and Higher Education and the National Science Centre, Poland; the Fundação para a Ciência e a Tecnologia, Portugal; JINR, Dubna; the Ministry of Education and Science of the Russian Federation, the Federal Agency of Atomic Energy of the Russian Federation, Russian Academy of Sciences, and the Russian Foundation for Basic Research; the Ministry of Education, Science and Technological Development of Serbia; the Secretaría de Estado de Investigación, Desarrollo e Innovación and Programa Consolider-Ingenio 2010, Spain; the Swiss Funding Agencies (ETH Board, ETH Zurich, PSI, SNF, UniZH, Canton Zurich, and SER); the Ministry of Science and Technology, Taipei; the Thailand Center of Excellence in Physics, the Institute for the Promotion of Teaching Science and Technology of Thailand, Special Task Force for Activating Research and the National Science and Technology Development Agency of Thailand; the Scientific and Technical Research Council of Turkey, and Turkish Atomic Energy Authority; the National Academy of Sciences of Ukraine, and State Fund for Fundamental Researches, Ukraine; the Science and Technology Facilities Council, UK; the US Department of Energy, and the US National Science Foundation. Individuals have received support from the Marie-Curie program and the European Research Council and EPLANET (European Union); the Leventis Foundation; the A. P. Sloan Foundation; the Alexander von Humboldt Foundation; the Belgian Federal Science Policy Office; the Fonds pour la Formation à la Recherche dans l'Industrie et dans l'Agriculture (FRIA-Belgium); the Agentschap voor Innovatie door Wetenschap en Technologie (IWT-Belgium); the Ministry of Education, Youth and Sports (MEYS) of the Czech Republic; the Council of Science and Industrial Research, India; the HOMING PLUS program of the Foundation for Polish Science, cofinanced from European Union, Regional Development Fund, the Mobility Plus program of the Ministry of Science and Higher Education, the National Science Center (Poland), contracts Harmonia 2014/14/M/ST2/00428, Opus 2013/11/B/ST2/04202, 2014/13/B/ST2/02543 and 2014/15/B/ST2/03998, Sonata-bis 2012/07/E/ST2/01406; the Thalis and Aristeia programs cofinanced by EU-ESF and the Greek NSRF; the National Priorities Research Program by Qatar National Research Fund; the Programa Clarín-COFUND del Principado de Asturias; the Rachadapisek Sompot Fund for Postdoctoral Fellowship, Chulalongkorn University and the Chulalongkorn Academic into Its 2nd Century Project Advancement Project (Thailand); and the Welch Foundation, contract C-1845.

References

[1] T. Matsui and H. Satz, "J/ψ suppression by quark-gluon plasma formation", *Phys. Lett. B* **178** (1986) 416, doi:10.1016/0370-2693(86)91404-8.

[2] NA50 Collaboration, "Evidence for deconfinement of quarks and gluons from the J/ψ suppression pattern measured in Pb-Pb collisions at the CERN-SPS", *Phys. Lett. B* **477** (2000) 28, doi:10.1016/S0370-2693(00)00237-9.

[3] NA60 Collaboration, "J/ψ production in indium-indium collisions at 158 GeV/nucleon", *Phys. Rev. Lett.* **99** (2007) 132302, doi:10.1103/PhysRevLett.99.132302, arXiv:0706.4361.

[4] PHENIX Collaboration, "J/ψ Production vs. Centrality, Transverse Momentum, and Rapidity in Au+Au Collisions at $\sqrt{s_{\mathrm{NN}}} = 200\,\mathrm{GeV}$", *Phys. Rev. Lett.* **98** (2007) 232301, doi:10.1103/PhysRevLett.98.232301, arXiv:nucl-ex/0611020.

[5] CMS Collaboration, "Suppression of non-prompt J/ψ, prompt J/ψ, and Y(1S) in PbPb collisions at $\sqrt{s_{\mathrm{NN}}} = 2.76\,\mathrm{TeV}$", *JHEP* **05** (2012) 063, doi:10.1007/JHEP05(2012)063, arXiv:1201.5069.

[6] ALICE Collaboration, "Centrality, rapidity and transverse momentum dependence of J/ψ suppression in Pb-Pb collisions at $\sqrt{s_{\mathrm{NN}}} = 2.76\,\mathrm{TeV}$", *Phys. Lett. B* **734** (2014) 314, doi:10.1016/j.physletb.2014.05.064, arXiv:1311.0214.

[7] CMS Collaboration, "Indications of suppression of excited Y states in PbPb collisions at $\sqrt{s_{\mathrm{NN}}} = 2.76\,\mathrm{TeV}$", *Phys. Rev. Lett.* **107** (2011) 052302, doi:10.1103/PhysRevLett.107.052302, arXiv:1105.4894.

[8] CMS Collaboration, "Observation of sequential Y suppression in PbPb collisions", *Phys. Rev. Lett.* **109** (2012) 222301, doi:10.1103/PhysRevLett.109.222301, arXiv:1208.2826.

[9] A. Emerick, X. Zhao, and R. Rapp, "Bottomonia in the Quark-Gluon Plasma and their Production at RHIC and LHC", *Eur. Phys. J. A* **48** (2012) 72, doi:10.1140/epja/i2012-12072-y, arXiv:1111.6537.

[10] M. Strickland and D. Bazow, "Thermal Bottomonium Suppression at RHIC and LHC", *Nucl. Phys. A* **879** (2012) 25, doi:10.1016/j.nuclphysa.2012.02.003, arXiv:1112.2761.

[11] E. Ferreiro, F. Fleuret, J. Lansberg, and A. Rakotozafindrabe, "Impact of the Nuclear Modification of the Gluon Densities on J/ψ production in p–Pb collisions at $\sqrt{s_{\mathrm{NN}}} = 5\,\mathrm{TeV}$", *Phys. Rev. C* **88** (2013) 047901, doi:10.1103/PhysRevC.88.047901, arXiv:1305.4569.

[12] R. Vogt, "Shadowing effects on J/ψ and Y production at energies available at the CERN Large Hadron Collider", *Phys. Rev. C* **92** (2015) 034909, doi:10.1103/PhysRevC.92.034909, arXiv:1507.04418.

[13] F. Arleo and S. Peigné, "J/ψ suppression in p-A collisions from parton energy loss in cold QCD matter", *Phys. Rev. Lett.* **109** (2012) 122301, doi:10.1103/PhysRevLett.109.122301, arXiv:1204.4609.

[14] F. Arleo, R. Kolevatov, S. Peigné, and M. Rustamova, "Centrality and $p_\perp$ dependence of J/ψ suppression in proton-nucleus collisions from parton energy loss", *JHEP* **05** (2013) 155, doi:10.1007/JHEP05(2013)155, arXiv:1304.0901.

[15] CMS Collaboration, "Study of B Meson Production in p+Pb Collisions at $\sqrt{s_{\rm NN}} = 5.02$ TeV Using Exclusive Hadronic Decays", *Phys. Rev. Lett.* **116** (2016) 032301, doi:10.1103/PhysRevLett.116.032301, arXiv:1508.06678.

[16] CMS Collaboration, "Transverse momentum spectra of inclusive b jets in pPb collisions at $\sqrt{s_{\rm NN}} = 5.02$ TeV", *Phys. Lett. B* **754** (2016) 59, doi:10.1016/j.physletb.2016.01.010, arXiv:1510.03373.

[17] ALICE Collaboration, "J/ψ production and nuclear effects in p-Pb collisions at $\sqrt{s_{\rm NN}} = 5.02$ TeV", *JHEP* **02** (2014) 073, doi:10.1007/JHEP02(2014)073, arXiv:1308.6726.

[18] ALICE Collaboration, "Rapidity and transverse-momentum dependence of the inclusive J/ψ nuclear modification factor in p-Pb collisions at $\sqrt{s_{\rm NN}} = 5.02$ TeV", *JHEP* **06** (2015) 055, doi:10.1007/JHEP06(2015)055, arXiv:1503.07179.

[19] ATLAS Collaboration, "Measurement of differential J/ψ production cross sections and forward-backward ratios in p+Pb collisions with the ATLAS detector", *Phys. Rev. C* **92** (2015) 034904, doi:10.1103/PhysRevC.92.034904, arXiv:1505.08141.

[20] LHCb Collaboration, "Study of J/ψ production and cold nuclear matter effects in pPb collisions at $\sqrt{s_{\rm NN}}$ =5 TeV", *JHEP* **02** (2014) 072, doi:10.1007/JHEP02(2014)072, arXiv:1308.6729.

[21] CMS Collaboration, "The CMS experiment at the CERN LHC", *JINST* **3** (2008) S08004, doi:10.1088/1748-0221/3/08/S08004.

[22] CMS Collaboration, "Multiplicity and transverse momentum dependence of two- and four-particle correlations in pPb and PbPb collisions", *Phys. Lett. B* **724** (2013) 213, doi:10.1016/j.physletb.2013.06.028, arXiv:1305.0609.

[23] CMS Collaboration, "Performance of CMS muon reconstruction in pp collision events at $\sqrt{s} = 7$ TeV", *JINST* **7** (2012) P10002, doi:10.1088/1748-0221/7/10/P10002, arXiv:1206.4071.

[24] T. Sjöstrand, S. Mrenna, and P. Skands, "PYTHIA 6.4 physics and manual", *JHEP* **05** (2006) 026, doi:10.1088/1126-6708/2006/05/026, arXiv:hep-ph/0603175.

[25] T. Sjöstrand et al., "An Introduction to PYTHIA 8.2", *Comput. Phys. Commun.* **191** (2015) 159, doi:10.1016/j.cpc.2015.01.024, arXiv:1410.3012.

[26] P. Bartalini and L. Fano, eds., "Proceedings, 1st International Workshop on Multiple Partonic Interactions at the LHC (MPI08)". (2010). arXiv:1003.4220.

[27] R. Field, "Early LHC Underlying Event Data — Findings and Surprises", in *Hadron collider physics. Proceedings, 22nd Conference, HCP 2010, Toronto, Canada, August 23-27.* 2010. arXiv:1010.3558.

[28] CMS Collaboration, "Measurement of the prompt J/ψ and $\psi(2S)$ polarizations in pp collisions at $\sqrt{s} = 7$ TeV", *Phys. Lett. B* **727** (2013) 381, doi:10.1016/j.physletb.2013.10.055, arXiv:1307.6070.

[29] D. J. Lange, "The EvtGen particle decay simulation package", *Nucl. Instrum. Meth. A* **462** (2001) 152, doi:10.1016/S0168-9002(01)00089-4.

[30] E. Barberio and Z. Was, "PHOTOS — A universal Monte Carlo for QED radiative corrections: version 2.0", *Comput. Phys. Commun.* **79** (1994) 291, doi:10.1016/0010-4655(94)90074-4.

[31] GEANT Collaboration, "GEANT4 — A simulation toolkit", *Nucl. Instrum. Meth. A* **506** (2003) 250, doi:10.1016/S0168-9002(03)01368-8.

[32] C. Patrignani and et al. (Particle Data Group), "Review of Particle Physics", *Chin. Phys. C* **40** (2016) 100001, doi:10.1088/1674-1137/40/10/100001.

[33] CMS Collaboration, "CMS Luminosity Calibration for the pp Reference Run at $\sqrt{s} = 5.02\,\text{TeV}$", CMS Physics Analysis Summary CMS-PAS-LUM-16-001, 2016.

[34] CMS Collaboration, "Luminosity calibration for the 2013 proton-lead and proton-proton data taking", CMS Physics Analysis Summary CMS-PAS-LUM-13-002, 2014.

[35] M. L. Miller, K. Reygers, S. J. Sanders, and P. Steinberg, "Glauber modeling in high-energy nuclear collisions", *Ann. Rev. Nucl. Part. Sci.* **57** (2007) 205, doi:10.1146/annurev.nucl.57.090506.123020, arXiv:nucl-ex/0701025.

[36] CMS Collaboration, "J/ψ and $\psi(2S)$ production in pp collisions at $\sqrt{s} = 7\,\text{TeV}$", *JHEP* **02** (2012) 011, doi:10.1007/JHEP02(2012)011, arXiv:1111.1557.

[37] CMS Collaboration, "Measurement of J/ψ and $\psi(2S)$ Prompt Double-Differential Cross Sections in pp Collisions at $\sqrt{s} = 7\,\text{TeV}$", *Phys. Rev. Lett.* **114** (2015) 191802, doi:10.1103/PhysRevLett.114.191802, arXiv:1502.04155.

[38] M. J. Oreglia, "A study of the reactions $\psi' \to \gamma\gamma\psi$". PhD thesis, Stanford University, 1980. SLAC Report SLAC-R-236.

[39] CMS Collaboration, "Measurements of Inclusive W and Z Cross Sections in pp Collisions at $\sqrt{s} = 7\,\text{TeV}$", *JHEP* **01** (2011) 080, doi:10.1007/JHEP01(2011)080, arXiv:1012.2466.

[40] X.-N. Wang and M. Gyulassy, "HIJING: A Monte Carlo model for multiple jet production in pp, pA and AA collisions", *Phys. Rev. D* **44** (1991) 3501, doi:10.1103/PhysRevD.44.3501.

[41] K. J. Eskola, H. Paukkunen, and C. A. Salgado, "EPS09: A New Generation of NLO and LO Nuclear Parton Distribution Functions", *JHEP* **04** (2009) 065, doi:10.1088/1126-6708/2009/04/065, arXiv:0902.4154.

[42] K. Kovařík et al., "nCTEQ15: Global analysis of nuclear parton distributions with uncertainties in the CTEQ framework", *Phys. Rev. D* **93** (2016) 085037, doi:10.1103/PhysRevD.93.085037, arXiv:1509.00792.

[43] J.-P. Lansberg and H.-S. Shao, "Towards an automated tool to evaluate the impact of the nuclear modification of the gluon density on quarkonium, D and B meson production in proton-nucleus collisions", arXiv:1610.05382.

[44] Z. Conesa del Valle et al., "Open-beauty production in pPb collisions at $\sqrt{s_{\text{NN}}} = 5\,\text{TeV}$: effect of the gluon nuclear densities", *Nucl. Phys. A* **926** (2014) 236, doi:10.1016/j.nuclphysa.2014.05.009, arXiv:1402.1747.